PAPER

Check for updates

Three resorcin[4]arene-based lanthanide-coordination polymers with multifunctional photoluminescence sensing properties†

Hang Zhang, [ID] *[a] Jia-Chen Wang,[a] Wei Jiang[b] and Si-Si Zhao*[a]

By utilizing a novel octacarboxylate-functionalized resorcin[4]arene as organic linkers, three lanthanide-coordination polymers, namely, $[(CH_3)_2NH_2][Ln_2(HL)(H_2O)_7] \cdot 2H_2O$ (Ln = Tb (**1**), Eu (**2**) and Gd (**3**), H_8L = 2,8,14,20-tetra-pentyl-4,6,10,12,16,18,22,24-octa-carboxymethoxy-resorcin[4]arene) have been solvothermally synthesized and structurally characterized. Isostructural **1–3** display unique two dimensional sandwich-based layers built with Ln^{3+} cations and bowl-shaped HL^{7-} anions. Remarkably, **1** and **2** produce intensive green and red emissions respectively and long lifetimes thanks to the antenna effect of HL^{7-} anions. The energy level testing of **3** indicates that the newly designed ligand H_8L has a very efficient intersystem crossing process. More importantly, luminescent investigations reveal that **1** and **2** can selectively detect N,N'-dimethylformamide and Fe^{3+} ions with turn-on-type and turn-off-type responses, respectively.

Introduction

Currently, probing hazardous chemicals, such as volatile organic compounds and metal ionic pollutants is of great importance because it is highly critical in the fields of biology, physiology, pharmacology and environmental sciences.[1–3] In light of the impacts that hazardous chemicals have on human health and the environment, developing effective technologies for the sensing of volatile organic compounds and metal ionic pollutants are therefore of global importance and highly necessary.[4,5] It needs to be mentioned that fluorometric techniques offer relative ease of use, technical simplicity, and wide applicability, and would likely be preferred during sensing of volatile organic compounds and metal ionic pollutants if available.[6,7]

Emerging as a class of luminescent materials, lanthanide-coordination polymers (Ln-CPs) have afforded a great opportunity in terms of molecular sensing because of their exceptional fluorescent features with narrow emission bands, long emission lifetimes, and high luminescent quantum efficiencies.[8–10] So far, fluorescent Ln-CPs have been successfully employed for luminescent sensing of harmful volatile organic

compounds, ionic pollutants, pH value, gas and biomarker molecules with a turn-off-type luminescent process.[11–14] Most recently, some progress has been achieved in development of turn-on-type Ln-CP luminescent sensors that were utilized to monitor local concentration fluctuations of environmentally hazardous chemicals.[15,16] However, single Ln-CP luminescent sensors that discriminate volatile organic compounds and metal ionic pollutants through different response types remain exceedingly rare.[17] Thus, it is an active and challenging research field to develop new luminescent Ln-CPs.

Among all lanthanide elements, Tb^{3+} and Eu^{3+} could show intense characteristic green and red emissions, respectively, when they are excited by energy transfer from an "antenna" linker to Ln^{3+} cations under UV irradiation.[18,19] Remarkably, during the probing process the bright color changes of green or red could even be observed by the naked eye directly.[20] On the other hand, introduction of suitable organic chromophoric sensitizers into Ln-CPs will significantly enhance the light absorption ability and increase the luminescent brightness of Ln^{3+} cations by "antennae effect".[21] In this regard, resorcin[4]arenes are particularly attractive because of their bodies and rims with various substituents, thus yielding a great diversity of ligands.[22,23] Thus far some metal–organic frameworks with fascinating structures and properties have been synthesized by applying the resorcin[4]arene-based ligands.[24,25] Remarkably, carboxylate-functionalized resorcin[4]arene ligands have been proven to exhibit strong "antennae effects" in building luminescent Ln-CPs.[26,27]

Based on above consideration, we herein report three Ln-CPs, namely, $[(CH_3)_2NH_2][Ln_2(HL)(H_2O)_7] \cdot 2H_2O$ [Ln = Tb (**1**), Eu (**2**), Gd (**3**)], assembled with a new octacarboxylate-

[a]Institute of Catalysis for Energy and Environment, College of Chemistry & Chemical Engineering, Shenyang Normal University, Shenyang, 110034, P. R. China. E-mail: zhangh@synu.edu.cn; zhaoss@synu.edu.cn

[b]College of Environmental Science and Engineering, Jilin Normal University, Siping, 136000, P. R. China

functionalized resorcin[4]arene ligand, 2,8,14,20-tetra-pentyl-4,6,10,12,16,18,22,24-octa-carboxymethoxy-resorcin[4]arene (H_8L) (Scheme 1). **1** and **2** emit unique and bright luminescence in visible light region. Most importantly, they could be applied as turn-on-type fluorescent sensors for N,N'-dimethylformamide (DMF) and exhibit selectively fluorescent turn-off responses triggered by Fe^{3+} ion in comparison to other ions.

Experimental

Materials and general measurements

Commercial chemicals were used as purchased unless otherwise mentioned. FT-IR spectra were determined on a Mattson Alpha Centauri spectrometer. Elemental analysis data were recorded on a Perkin-Elmer Model 240C elemental analyzer. Powder X-ray diffraction (PXRD) patterns were determined on a Rigaku Dmax 2000 X-ray diffractometer using CuKα radiation ($\lambda = 0.154$ nm). UV-vis spectra were measured on a Cary TU-1900 doublebeam UV-vis spectrophotometer. Thermogravimetric (TG) data were conducted on a Perkin-Elmer Model TG-7 analyzer under nitrogen gas. Luminescent spectra were performed on a FLSP920 Edinburgh Fluorescence Spectrometer.

Synthesis of H_8L

The precursor 1,3-bis[(methoxycarbonyl)methoxy]benzene (L1) was synthesized according to the literature procedure.[28] A mixture of L1 (2.56 g, 10.0 mmol) and hexaldehyde (1.0 g, 10 mmol) in dichloromethane (30 mL) was stirred at ice bath for 0.5 h with dropwise addition of $BF_3 \cdot OEt_2$ (6 mL). Then the mixture was stirred at room temperature overnight. The generated solid was collected and washed using CH_2Cl_2 to give L2 in a yield of 58%. Then sodium hydroxide (1.6 g, 40 mmol), tetrahydrofuran (150 mL), and water (150 mL) were added into L2. The solvents were removed by water bath, and then 100 mL water was added. The pH value of the mixture was adjusted to 1–2 by using HCl (1.0 mol L^{-1}), and solid H_8L was achieved in a 64% yield. Anal. calcd. for $C_{64}H_{80}O_{24}$ (Mr = 1232.50): C, 62.33; H, 6.54; N, 0.00. Found: C, 62.42; H, 6.47; N, 0.00. IR data (KBr, cm^{-1}) for H_8L: 3404(s), 2954(m), 2929(w), 2859(m), 2657(w), 2554(w), 1737(w), 1611(s), 1586(s), 1501(w), 1432(m), 1378(m), 1292(m), 1242(s), 1187(s), 1123(s), 1098(s), 1071(s), 972(s), 907(s), 822(s), 726(s), 673(s), 516(s).

Synthesis of $[(CH_3)_2NH_2][Tb_2(HL)(H_2O)_7] \cdot 2H_2O$ (1)

A mixture of H_8L (27.0 mg, 0.1 mmol) and $TbCl_3 \cdot 6H_2O$ (18.0 mg, 0.048 mmol) was dissolved in a mixed solution of DMF (2 mL) and water (6 mL). Then the suspension was transferred into a Teflon-lined autoclave (15 mL) and heated at 100 °C for 3 days. Colorless crystals of **1** were achieved in a 35% yield based on Tb^{3+} after cooling the reactor to room temperature. Anal. calcd. for $C_{66}H_{94}Tb_2NO_{33}$ (Mr = 1747.26): C, 45.36; H, 5.42; N, 0.80. Found: C, 45.82; H, 5.60; N, 0.82. IR data (KBr, cm^{-1}): 3750(s), 3525(s), 3325(m), 3249(m), 2929(w), 2856(m), 1711(m), 1583(w), 1507(w), 1454(w), 1427(w), 1375(m), 1331(m), 1298(w), 1257(m), 1188(m), 1119(w), 1071(m), 939(s), 908(s), 852(s), 775(s), 725(m), 680(m), 582(s), 510(s), 413(s).

Synthesis of $[(CH_3)_2NH_2][Eu_2(HL)(H_2O)_7] \cdot 2H_2O$ (2) and $[(CH_3)_2NH_2][Gd_2(HL)(H_2O)_7] \cdot 2H_2O$ (3)

2 and **3** were synthesized in a similar procedure as **1**, in which $TbCl_3 \cdot 6H_2O$ was replaced by $EuCl_3 \cdot 6H_2O$ (17.0 mg, 0.048 mmol) and $GdCl_3 \cdot 6H_2O$ (18.0 mg, 0.048 mmol), respectively. Colorless crystals of **2** and **3** were achieved in 39% and 42% yields, respectively, based on Ln^{3+} cations. Anal. calcd. for $C_{66}H_{94}Eu_2NO_{33}$ (Mr = 1733.34): C, 45.73; H, 5.46; N, 0.80. Found: C, 45.66; H, 5.88; N, 0.85. IR data (KBr, cm^{-1}) for **2**: 3855(s), 3352(m), 2926(w), 2855(m), 1708(m), 1583(w), 1509(w), 1452(w), 1425(w), 1372(s), 1285(w), 1190(m), 1165(s), 1119(m), 1064(m), 962(s), 919(s), 848(s), 720(s), 639(s), 590(s). Anal. calcd. for $C_{66}H_{94}Gd_2NO_{33}$ (Mr = 1743.92): C, 45.45; H, 5.43; N, 0.80. Found: C, 45.30; H, 5.71; N, 0.84. IR data (KBr, cm^{-1}) for **3**: 3750(s), 3369(m), 2929(w), 2857(m), 1578(w), 1508(w), 1427(w), 1376(s), 1332 (s), 1295(w), 1189(m), 1120(m), 1071(m), 959(s), 919(s), 848(s), 726(s), 678(s), 584(s), 413(s).

Luminescent sensing experiments

Before luminescent determination, the samples of Ln-CPs were ground into powder. Then the suspension was prepared by introducing the powder sample (3 mg) of Ln-CPs into each volatile organic compounds solvent (3 mL) or stock solutions (1 $\times 10^{-2}$ M, 3 mL) of MCl_x by ultrasound treatment for 1 min. Each suspension was transferred to a cuvette and tested by luminescent spectrum.

Measurement for luminescent sensing of DMF vapor

A small beaker (10 mL) with the samples (10 mg) was placed into a big sealed container (50 mL) with DMF (20 mL) for 24 h or 10 min. Subsequently, the small beaker was taken out from the container and quickly sealed, and the emission spectra were measured by using the solid samples. The initial emission spectrum of the solid sample was measured in a solid sample holder before exposure to DMF vapor.

X-ray crystallography

Crystallographic data for **1–3** were determined on an Oxford Diffraction Gemini R Ultra diffractometer using graphite-monochromated Mo-Kα radiation ($\lambda = 0.71073$ Å). The structure were solved by direct method and refined on F^2 by full-

Scheme 1 Synthetic route of the resorcin[4]arene-based H_8L ligand.

matrix least-squares method using the SHELXL-97 within WINGX.[29-31] H atoms of the organic molecules were placed geometrically. Further crystallographic details are listed in Table S1.† Selected bond lengths and angles for **1–3** are listed in Tables S2–S4.†

Results and discussion

Crystal structural descriptions of $[(CH_3)_2NH_2][Tb_2(HL)(H_2O)_7]\cdot 2H_2O$ (1), $[(CH_3)_2NH_2][Eu_2(HL)(H_2O)_7]\cdot 2H_2O$ (2) and $[(CH_3)_2NH_2][Gd_2(HL)(H_2O)_7]\cdot 2H_2O$ (3)

1–3 are isostructural and crystallize in the same triclinic space group $P\bar{1}$. Herein, we will only describe the structure of **1** in detail (Fig. S1†). One of the most striking features of such Ln-CPs is the presence of numerous coordinated waters around the Ln^{3+} centers. The asymmetric unit of **1** consists of two Tb^{3+} cations, one HL^{7-} anion, seven coordinated water molecules, one $[H_2N(CH_3)_2]^+$ cation, and two lattice water molecules (Fig. 1a). Two Tb^{3+} cations exhibit different coordination spheres. Tb1 is in a distorted square antiprism geometry, surrounded by eight oxygen atoms from two different HL^{7-} anions and three coordinated water molecules. Tb2 is coordinated by nine oxygen atoms from three HL^{7-} anions and four coordinated water molecules in a distorted tricapped trigonal prism sphere. The Tb–O bond distances vary from 2.300(14) to 2.648(17) Å, which are within the normal range.[32] One $[H_2N(CH_3)_2]^+$ cation is included as a counter cation to balance the negative charge. Seven carboxylates of each HL^{7-} anion are involved in coordination with five Tb^{3+} cations. It is noticeable that two HL^{7-} anions form a sandwich-like unit *via* sharing two Tb1 cations (Fig. 1b). Further, adjacent sandwich-like units are interconnected by Tb2 cations to give a unique two dimensional sandwich-based layer (Fig. 1c).

Luminescent properties

Solid state emission spectra of the free H_8L and **1** and **2** were determined at room temperature. For the free H_8L, the emission peak at 366 nm ($\lambda_{ex} = 315$ nm) corresponds to the $\pi^* \rightarrow \pi$ or $\pi^* \rightarrow n$ transitions,[33] as shown in Fig. S2.† When excited at 295 nm, **1** emits characteristic emission peaks at 488, 543, 584, and 623 nm, which could be ascribed to $^5D_4 \rightarrow {}^7F_J$ ($J = 6$–3) transitions of the Tb^{3+} cations (Fig. 2a).[30] The most intense emission at 543 nm is attributed to the $^5D_4 \rightarrow {}^7F_5$ transition of the Tb^{3+} cations, resulting in an intense green emission output in the solid state.[34] Similarly, **2** exhibits characteristic transitions of the Eu^{3+} cations upon excitation at 318 nm. As depicted in Fig. 2b, the emission peaks at 579, 593, 614, 651, and 698 nm correspond to the $^5D_0 \rightarrow {}^7F_J$ ($J = 0$–4) transitions of the Eu^{3+} cations.[35] Notably, the emission spectrum of **2** is mainly dominated by the $^5D_0 \rightarrow {}^7F_2$ transition, which is more intense than others, leading to intense red luminescence.[36] The bright colors also demonstrate that HL^{7-} acts as an excellent "antenna" linker in the effectively transfer energies to Tb^{3+} and Eu^{3+} metals.[37]

Another critical luminescence characteristic of Ln-CPs is the lifetime, which refers to the average time that a molecule stays in its excited state before emitting a photon.[38] Hence, the lifetime values of the excited states $^5D_4$ (Tb^{3+}) and $^5D_0$ (Eu^{3+}) of **1** and **2** were monitored with 543 and 614 nm, respectively (Fig. S3†). The observed luminescent decay profiles correspond to single exponential functions, with the lifetimes of $\tau = 0.730$ ms for **1** and $\tau = 1.242$ ms for **2**.[39] Moreover, the ligand-centered emission is not detected, thus implying the existence of an efficient ligand-to-metal energy-transfer process in these Ln-CPs.[40]

To better understand the energy transfer process, the UV-vis absorption spectrum of **3** was determined in methanol solution at room temperature.[41] The wavelength of the absorbance edge is about 312 nm, indicating that HL^{7-} has a singlet state (S1) energy level of 32 051 cm^{-1} (Fig. S4a†). The phosphorescent spectrum of **3** was also recorded at 77 K to estimate the triplet state (T1) energy level of HL^{7-}, and obtained the T1 energy level of 22 675 cm^{-1} (Fig. S4b†). According to Reinhoudt's empirical rule, the energy transfer from ligand to metal will become effective when the energy gap between S1 and T1 of the organic
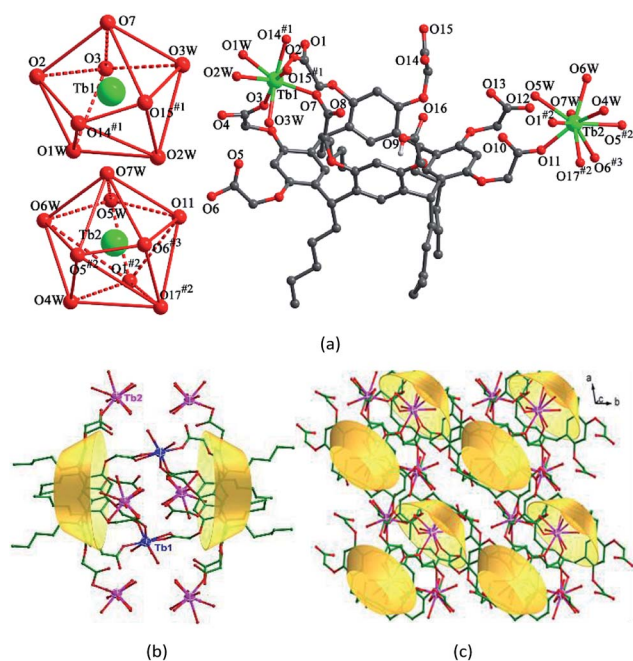

Fig. 1 (a) Coordination environments of Tb^{3+} cations in **1**. (b) View of the sandwich unit of **1**. (c) Top view of the unique 2D sandwich-based network of **1**.
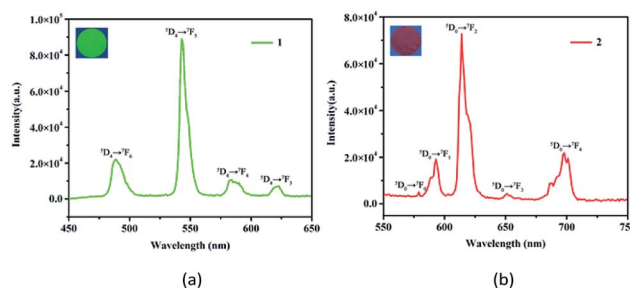

Fig. 2 Solid state emission spectra and luminescent images of **1** (a) and **2** (b).

Scheme 2 Energy level scheme showing energy transfer processes in **1** and **2**.

linker is at least 5000 cm^{-1}.[41] For HL^{7-}, the energy gap between S1 and T1 is 9376 cm^{-1}, implying that the intersystem crossing process is greatly efficient. Generally, to fulfill luminescent Tb- and Eu-CP sensors, the organic ligands should have a suitable T1 in 22 000–27 000 cm^{-1} to well match their energy levels ($^5D_4$, 20 500 cm^{-1} for Tb^{3+}, and $^5D_0$, 17 500 cm^{-1} for Eu^{3+}).[42] In our case, the T1 energy level of HL^{7-} is 22 675 cm^{-1}, indicating that HL^{7-} could efficiently sensitize both Eu^{3+} and Tb^{3+} emissions.[42] The energy transfer process illustrated in Scheme 2 shows ligand-to-metal energy transfers.

Luminescent recognition of DMF

Most recently, volatile organic compounds sensing has gained considerable interest in fundamental and practical research due to their potential applications in optical devices, environmental monitoring, and separation.[43,44] To explore the potential applications in this field, luminescent responses of **1** and **2** after incubation in various volatile organic compounds, including chloroform, dichloromethane, ethanol, acetonitrile, tetrahydrofuran, ether, cyclohexane, methanol and DMF, were studied in detail. As shown in Fig. 3, the corresponding luminescence curves still show the four characteristic emission peaks, and only the relative $^5D_4 \to {}^7F_5$ or $^5D_0 \to {}^7F_2$ transition intensities of **1** and **2** were monitored under the perturbation of various volatile organic compounds. Particularly, DMF triggers a superior luminescent turn-on effect for **1** and **2**, while other volatile organic compounds have no significant effect on the emission. Moreover, the inset photographs shows that only DMF can obviously enhance the emission colors of **1** and **2**, which leads to brighten under UV light. This finding suggests that **1** and **2** are potential sensing materials for DMF with an excellent selectivity.

The obvious emission intensity enhancement of **1** and **2** by displacement in DMF encouraged us to further explore the potential applications of them for probing DMF vapor. In order to test the performance of **1** and **2** as DMF vapor sensor, an *in situ* solid-state luminescent sensor setup was designed and used (Fig. S5†). The luminescence response of **1** and **2** after incubation for 24 h under DMF vapor were measured and the results are plotted in Fig. 4. The observation indicates **1** and **2** still exhibit a clear enhancement effect. Besides good sensitivity, fast response is also an important criterion for a good sensor. Hence, the solid state emission spectra of **1** and **2** were further determined after exposed in DMF vapor for 10 minutes. Clearly, the response rate of
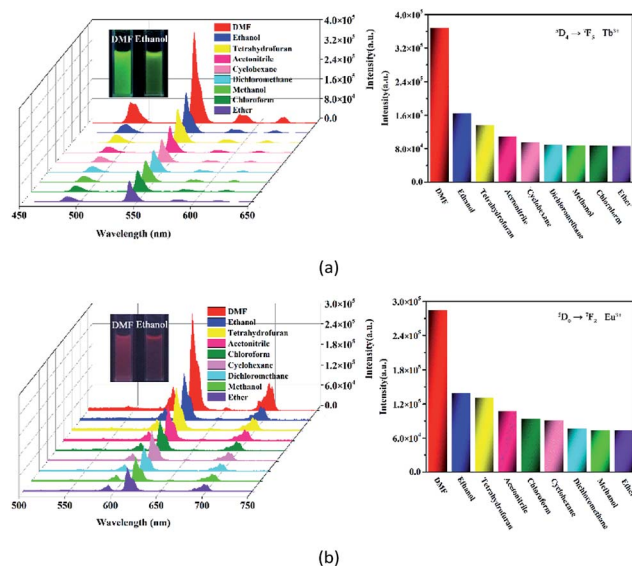

(a)

(b)

Fig. 3 Emission spectra and the relative $^5D_4 \to {}^7F_5$ or $^5D_0 \to {}^7F_2$ transition intensities of **1** (a) and **2** (b) in various volatile organic compounds upon excitation at 295 and 318 nm, respectively (the inset photographs show the colors for **1** and **2** dispersed in DMF (left) and ethanol (right) under a UV light (λ_{ex} = 365 nm)).

the sensor is quite fast with 88.9% and 89.7% (the relative $^5D_4 \to {}^7F_5$ or $^5D_0 \to {}^7F_2$ transition intensities) of enhancement achieved compared that after 24 h, rendering **1** and **2** potential sensors for turn-on-type detection of DMF vapor. Moreover, PXRD patterns of **1** and **2** in DMF vapor are nearly identical to the simulated one, suggesting they are stable in the luminescent sensing process (Fig. S6†).

The emission intensity of the Ln^{3+} is well-known to rely on the energy transfer efficiency from the ligand to the Ln^{3+} center.[45] Meanwhile, the interactions with the O–H bond of coordinated water may lead to quenching of Ln^{3+} luminescence.[45] DMF has a more strong coordination ability compared to other volatile organic compound. When coordinated waters are partially changed by DMF, the O–H bonds surrounding the Ln^{3+} centers may leave fewer and thus enhance Ln^{3+} emission. Hence, we infer that the marked enhancement of their emission intensities in response to DMF is likely caused by the displacement of coordinated water molecules by DMF molecules.

Selective sensing of Fe^{3+} ion

Metal ion sensing and detection play a significant role in environment and life science.[46–48] In this study, we also investigated
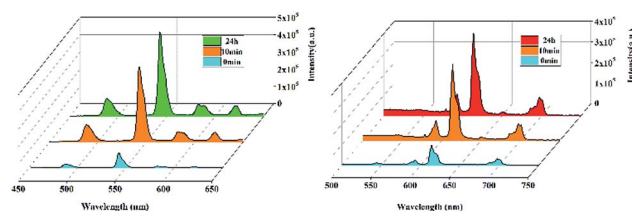

Fig. 4 Luminescent intensity for **1** and **2** upon exposure to DMF vapor at different time.

luminescent **1** and **2** to sense metal ionic pollutants. The crystalline samples were simply soaked in aqueous solutions of MCl_x (M = Na^+, K^+, Ca^{2+}, Cd^{2+}, Zn^{2+}, Mn^{2+}, Ni^{2+}, Mg^{2+}, Co^{2+}, Al^{3+}, Cu^{2+}, Cr^{3+} Fe^{2+} and Fe^{3+}, 1×10^{-2} M) for luminescence studies. As depicted in Fig. 5, the corresponding luminescence curves still show the four characteristic emission peaks, and only the relative $^5D_4 \rightarrow {}^7F_5$ or $^5D_0 \rightarrow {}^7F_2$ transition intensities for **1** and **2** were monitored under the perturbation of various cations. Interestingly, Fe^{3+} exhibits a pronounced quenching effect on the luminescence of **1** and **2**, while other metal ions have no significant effect with the exception of Fe^{2+} or Cr^{3+}, which can weaken the luminescence to some extent. Moreover, the inset photographs show that only Fe^{3+} can completely quench the emission colors of **1** and **2**, which leads to the dark under UV light. The above phenomenon indicate that **1** and **2** may be considered as a promising luminescent probe for Fe^{3+} ions.

To further prove the luminescent quenching by Fe^{3+} ion, concentration-dependent luminescent studies for **1** and **2** were carried out in the presence of Fe^{3+} ion. As demonstrated in Fig. 6, the emission intensity for the suspension of **1** and **2** sharply declines with the increase of Fe^{3+} concentration from 0 to 5000 μM. At the Fe^{3+} content of 5×10^{-3} M, the fluorescence intensity of **1** and **2** completely disappeared. Quantitatively, the Stern–Volmer equation $I_0/I = 1 + K_{sv}[M]$ can be used to describe this quenching effect, where the values I_0 and I represent the luminescent intensities of **1** without and with addition of Fe^{3+}, respectively, [M] is the concentration of Fe^{3+}, and K_{sv} is the quenching constant. Based on the quenching experimental data, the K_{sv} value is calculated to be 1.545×10^4, suggesting a strong quenching effect on the luminescence of **1**. The calculated linear correlation coefficient (R) in the K_{sv} curve of **1** with addition of Fe^{3+} is 0.99685, demonstrating that the quenching effect of Fe^{3+} on the luminescence of **1** fits the Stern–

Fig. 6 Emission spectra and linear relationship for **1** in aqueous solution of different concentrations of Fe^{3+}.

Volmer model. The suspension of **2** also exhibits the similar selective sensing of Fe^{3+} ion. The calculated K_{sv} value is 3.93×10^4 based on the Stern–Volmer equation, demonstrating a quenching effect on the fluorescence of **2**. Besides, a good linear relationship is achieved with the coefficient of 0.96502 (Fig. S7†).

To understand the mechanism of the fluorescence quenching effect of **1** and **2** toward Fe^{3+} ions the UV/vis absorption data of **1** and **2** and varied metal ions were carried out. The UV/vis absorption spectra show that the wide absorption band from 260 to 400 nm of Fe^{3+} covers the range of absorption bands of **1** and **2**, and is much more stronger than those of other metal ions (Fig. S8†). This means that the UV/vis absorption of Fe^{3+} upon excitation may prevent the absorption of **1** and **2**, and result in the decrease or quenching of the luminescence.[49,50]

Conclusions

In summary, we reported three Ln-CPs assembled with a new octacarboxylate-functionalized resorcin[4]arene ligand and Ln^{3+} cations. **1** and **2** emit intense characteristic red and green emission colors. The photophysical properties demonstrated that H_8L is well suited for the sensitization of Tb^{3+} and Eu^{3+} emissions thanks to the favorable energy level of its triplet state. **1** and **2** could be employed as potential turn-on-type fluorescent sensors for DMF and turn-off-type luminescent probe for Fe^{3+} ion.

Conflicts of interest

There are no conflicts to declare.

Acknowledgements

Notes and references

1 H. Wang, W. P. Lustig and J. Li, *Chem. Soc. Rev.*, 2018, **47**, 4729–4756.

2 D. Wu, A. C. Sedgwick, T. Gunnlaugsson, E. U. Akkaya, J. Yoon and T. D. James, *Chem. Soc. Rev.*, 2017, **46**, 7105–7123.
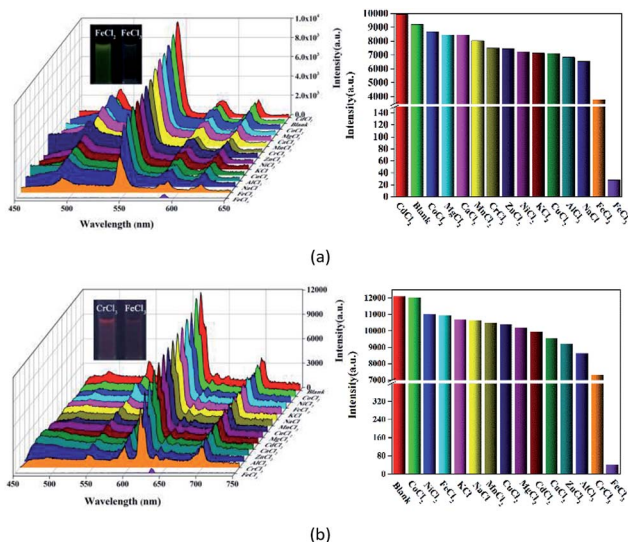

Fig. 5 Emission spectra and the relative $^5D_4 \rightarrow {}^7F_5$ or $^5D_0 \rightarrow {}^7F_2$ transition intensities of **1** (a) and **2** (b) in various aqueous solutions of MCl_x upon excitation at 295 and 318 nm, respectively (the inset photographs show the colors for **1** and **2** dispersed in aqueous solutions of $FeCl_2/CrCl_3$ (left) and $FeCl_3$ (right) under a UV light ($\lambda_{ex} = 365$ nm)).

3 B. Wang, X. L. Lv, D. Feng, L. H. Xie, J. Zhang, M. Li, Y. Xie, J. R. Li and H. C. Zhou, *J. Am. Chem. Soc.*, 2016, **138**, 6204–6216.

4 Y. Zhang, S. Yuan, G. Day, X. Wang, X. Yang and H.-C. Zhou, *Coord. Chem. Rev.*, 2018, **354**, 28–45.

5 X. L. Yang, X. Chen, G. H. Hou, R. F. Guan, R. Shao and M. H. Xie, *Adv. Funct. Mater.*, 2016, **26**, 393–398.

6 W. P. Lustig, S. Mukherjee, N. D. Rudd, A. V. Desai, J. Li and S. K. Ghosh, *Chem. Soc. Rev.*, 2017, **46**, 3242–3285.

7 M. Rieger, M. Wittek, P. Scherer, S. Löbbecke and K. Müller-Buschbaum, *Adv. Funct. Mater.*, 2018, **28**, 1704250.

8 Y. Cui, J. Zhang, H. He and G. Qian, *Chem. Soc. Rev.*, 2018, **47**, 5740–5785.

9 T. N. Nguyen, G. Capano, A. Gładysiak, F. M. Ebrahim, S. V. Eliseeva, A. Chidambaram, B. Valizadeh, S. Petoud, B. Smit and K. C. Stylianou, *Chem. Commun.*, 2018, **54**, 6816–6819.

10 C. Y. Chow, S. V. Eliseeva, E. R. Trivedi, T. N. Nguyen, J. W. Kampf, S. Petoud and V. L. Pecoraro, *J. Am. Chem. Soc.*, 2016, **138**, 5100–5109.

11 S. Wu, Y. Lin, J. Liu, W. Shi, G. Yang and P. Cheng, *Adv. Funct. Mater.*, 2018, **28**, 1707169.

12 J. N. Hao and B. Yan, *Nanoscale*, 2016, **8**, 12047–12053.

13 B. Yan, *Acc. Chem. Res.*, 2017, **50**, 2789–2798.

14 L. Li, J. Cheng, Z. Liu, L. Song, Y. You, X. Zhou and W. Huang, *ACS Appl. Mater. Interfaces*, 2018, **10**, 44109–44115.

15 P. Harvey, A. Nonat, C. Platas-Iglesias, L. S. Natrajan and L. J. CharbonniHre, *Angew. Chem., Int. Ed.*, 2018, **57**, 9921–9924.

16 B. Liu, H. Shen, Y. Hao, X. Zhu, S. Li, Y. Huang, P. Qu and M. Xu, *Anal. Chem.*, 2018, **90**, 12449–12455.

17 S. Anbu, R. Ravishankaran, M. F. C. G. da Silva, A. A. Karande and A. J. L. Pombeiro, *Inorg. Chem.*, 2014, **53**, 6655–6664.

18 R. F. Bogale, Y. Chen, J. Ye, Y. Yang, A. Rauf, L. Duan, P. Tian and G. Ning, *Sens. Actuators, B*, 2017, **245**, 171–178.

19 S. N. Zhao, L. J. Li, X. Z. Song, M. Zhu, Z. M. Hao, X. Meng, L. L. Wu, J. Feng, S. Y. Song, C. Wang and H. J. Zhang, *Adv. Funct. Mater.*, 2015, **25**, 1463–1469.

20 D. Zhao, D. Yue, L. Zhang, K. Jiang and G. Qian, *Inorg. Chem.*, 2018, **57**, 12596–12602.

21 Q. Zhang, J. Wang, A. M. Kirillov, W. Dou, C. Xu, C. Xu, L. Yang, R. Fang and W. Liu, *ACS Appl. Mater. Interfaces*, 2018, **10**, 23976–23986.

22 B.-B. Lu, W. Jiang, J. Yang, Y.-Y. Liu and J.-F. Ma, *ACS Appl. Mater. Interfaces*, 2017, **9**, 39441–39449.

23 Q.-Y. Zhai, J. Su, T.-T. Guo, J. Yang, J.-F. Ma and J.-S. Chen, *Cryst. Growth Des.*, 2018, **18**, 6046–6053.

24 W.-Y. Pei, G. Xu, J. Yang, H. Wu, B. Chen, W. Zhou and J.-F. Ma, *J. Am. Chem. Soc.*, 2017, **139**, 7648–7656.

25 B.-B. Lu, J. Yang, G.-B. Che, W.-Y. Pei and J.-F. Ma, *ACS Appl. Mater. Interfaces*, 2018, **10**, 2628–2636.

26 S. T. Zhang, J. Yang, H. Wu, Y. Y. Liu and J. F. Ma, *Chem.–Eur. J.*, 2015, **21**, 15806–15819.

27 X. Han, J. Yang, Y.-Y. Liu and J.-F. Ma, *Dyes Pigm.*, 2019, **160**, 492–500.

28 H. Zhang, J. Yang, Y. Y. Liu, S. Song and J. F. Ma, *Cryst. Growth Des.*, 2016, **16**, 3244–3255.

29 G. M. Sheldrick, *SHELXS-97, programs for X-ray crystal structure solution*, University of Göttingen, Göttingen, Germany, 1997.

30 G. M. Sheldrick, *SHELXL-97, programs for X-ray crystal structure refinement*, University of Göttingen, Göttingen, Germany, 1997.

31 L. J. Farrugia, *WINGX, a windows program for Crystal Structure Analysis*, University of Glasgow, Glasgow, UK, 1988.

32 P. Wu, J. Wang, Y. Li, C. He, Z. Xie and C. Duan, *Adv. Funct. Mater.*, 2011, **21**, 2788–2794.

33 P. P. Cui, P. Zhao, X. D. Zhang, P. Wang and W. Y. Sun, *Dyes Pigm.*, 2016, **124**, 241–248.

34 Y. Cui, B. Chen and G. Qian, *Coord. Chem. Rev.*, 2014, **273**, 76–86.

35 J. Sahoo, R. Arunachalam, P. S. Subramanian, E. Suresh, A. Valkonen, K. Rissanen and M. Albrecht, *Angew. Chem., Int. Ed.*, 2016, **55**, 9625–9629.

36 A. D. Bettencourt-Dias, P. S. Barber and S. Bauer, *J. Am. Chem. Soc.*, 2012, **134**, 6987–6994.

37 W. Wang, R. Wang, Y. Ge and B. Wu, *RSC Adv.*, 2018, **8**, 42100–42108.

38 D. Ananias, F. A. A. Paz, D. S. Yufit, L. D. Carlos and J. Rocha, *J. Am. Chem. Soc.*, 2015, **137**, 3051–3058.

39 C.-L. Tao, Y.-M. Ying, H. Wang, B. Chen, G.-P. Zhu, Y.-J. Song, X.-G. Liu, Z. Zhao, L. Shen and B. Z. Tang, *J. Mater. Chem. C*, 2018, **6**, 12371–12376.

40 C. Zhan, S. Ou, C. Zou, M. Zhao and C. D. Wu, *Anal. Chem.*, 2014, **86**, 6648–6653.

41 C. Gao, A. M. Kirillov, W. Dou, X. Tang, L. Liu, X. Yan, Y. Xie, P. Zang, W. Liu and Y. Tang, *Inorg. Chem.*, 2014, **53**, 935–942.

42 J. M. Zhou, H. H. Li, H. Zhang, H. M. Li, W. Shi and P. Cheng, *Adv. Mater.*, 2015, **27**, 7072–7077.

43 X. Yan, H. Wang, C. E. Hauke, T. R. Cook, M. Wang, M. L. Saha, Z. X. Zhou, M. M. Zhang, X. P. Li, F. H. Huang and P. J. Stang, *J. Am. Chem. Soc.*, 2015, **137**, 15276–15286.

44 S. Rochat and T. M. Swager, *Angew. Chem., Int. Ed.*, 2014, **53**, 9792–9796.

45 Y. Li, S. Zhang and D. Song, *Angew. Chem., Int. Ed.*, 2013, **52**, 710–713.

46 H. Xu, H.-C. Hu, C.-S. Cao and B. Zhao, *Inorg. Chem.*, 2015, **54**, 4585–4587.

47 S.-Q. Lu, Y.-Y. Liu, Z.-M. Duan, Z.-X. Wang, M.-X. Li and X. He, *Cryst. Growth Des.*, 2018, **18**, 4602–4610.

48 Q. Zhang, J. Wang, A. M. Kirillov, W. Dou, C. Xu, L. Yang, R. Fang and W. Liu, *ACS Appl. Mater. Interfaces*, 2018, **10**, 23976–23986.

49 D. Zhao, X.-H. Liu, Y. Zhao, P. Wang, Y. Liu, M. Azam, S. I. Al-Resayes, Y. Lu and W.-Y. Sun, *J. Mater. Chem. A*, 2017, **5**, 15797–15807.

50 S.-S. Zhao, J. Yang, Y.-Y. Liu and J.-F. Ma, *Inorg. Chem.*, 2016, **55**, 2261–2273.